

THE EFFECT OF BIDIRECTIONAL FLOW ON TIDAL CHANNEL PLANFORMS

SERGIO FAGHERAZZI^{1*}, EMMANUEL J. GABET² AND DAVID JON FURBISH³

¹ Department of Geological Sciences and School of Computational Science and Information Technology, Florida State University, Tallahassee, Florida 32306-4120, USA

² Department of Geology, University of Montana, Missoula, Montana 59812-1296, USA

³ Department of Geological Sciences and Geophysical Fluid Dynamics Institute, Florida State University, Tallahassee, Florida 32306-4100, USA

Received 5 March 2002; Revised 6 March 2003; Accepted 25 March 2003

ABSTRACT

Salt marsh tidal channels are highly sinuous. For this project, field surveys and aerial photographs were used to characterize the planform of tidal channels at China Camp Marsh in the San Francisco Bay, California. To model the planform evolution, we assume that the topographic curvature of the channel centreline is a key element driving meander migration. Extraction of curvature data from a planimetric survey, however, presents certain problems because simple calculations based on equally distanced points on the channel axis produce numerical noise that pollutes the final curvature data. We found that a spline interpolation and a polynomial fit to the survey data provided us with a robust means of calculating channel curvature. The curvature calculations, combined with data from numerous cross-sections along the tidal channel, were used to parameterize a computer model. With this model, based on recent theoretical work, the relationship between planform shape and meander migration as well as the consequences of bidirectional flow on planform evolution have been investigated. Bank failure in vegetated salt marsh channels is characterized by slump blocks that persist in the channel for several years. It is therefore possible to identify reaches of active bank erosion and test model predictions. Our results suggest that the geometry and evolution of meanders at China Camp Marsh, California, reflect the ebb-dominated regime. Copyright © 2004 John Wiley & Sons, Ltd.

KEY WORDS: tide; tidal channel; salt marsh; meanders; bank erosion

INTRODUCTION

Salt marsh tidal channels are highly sinuous, forming complex dendritic networks (Fagherazzi *et al.*, 1999; Fagherazzi and Furbish, 2001). In fluvial rivers, the leading process in meander development is the redistribution of momentum created by channel curvature (Ikeda *et al.*, 1981). Flow momentum becomes concentrated on the outer bank, causing erosion and concomitant deposition on the inside bank, leading to point bar growth. The momentum redistribution and consequent secondary flow are sufficient explanation for meander formation (Ikeda *et al.* 1981; Blondeaux and Seminara, 1985). Furthermore, Blondeaux and Seminara (1985), and Seminara and Tubino (1992) demonstrated that alternate bars can trigger the formation of meander bends at the initial stages of meander development.

Tidal meanders have a cross-sectional morphology similar to terrestrial channels, with point bars on the inner bank and deeper flow on the outer bank. Barwis (1978) studied the morphology of intertidal point bars in a South Carolina marsh creek system and demonstrated that the geometry of these bars is determined by the ebb-dominated tidal current and the radius of curvature. Ebb dominance causes all point bars to be skewed toward the inner bank from the ebb side of the meander. For gentle meanders, point bars resemble bars in terrestrial channels, whereas for meanders with intermediate curvature the bidirectional tidal flow creates complex multilobed bars with flood-dominant chutes and interlobe ramps.

Distinct flood and ebb channels are also frequent in the sandy tidal flats in the Netherlands, where mutual evasion of flood and ebb channels (i.e. the flow during ebb and flood takes two different ways) occurs by means of flank chutes (van Veen, 1950; Geyl, 1976).

* Correspondence to: S. Fagherazzi, School of Computational Science and Information Technology, Dirac Science Library, Florida State University, Tallahassee, FL 31306-4120, USA. E-mail: sergio@csit.fsu.edu

In estuaries where the velocity of both currents is approximately the same, the shift in the line of highest velocity leads the ebb and the flood to erode opposite banks, creating a meander that is narrow at the bend apices and wide between bends (Ahnert, 1960). Bidirectional flow is thus a unique characteristic of tidal channels and leads to a planform morphology distinct from terrestrial rivers.

In salt marsh creeks the flow velocity has two peaks, during ebb and flood respectively. As observed by Bayliss-Smith *et al.* (1979), Leopold *et al.* (1993), Myrick and Leopold (1963), Healey *et al.* (1981) and Green *et al.* (1986), the two velocity peaks are not identical and occur at different water stages, producing the characteristic velocity asymmetry. This velocity asymmetry is a direct consequence of over-marsh flow, with a flood peak occurring for water elevation higher than the marsh surface and ebb peak for water depths below bankfull (Bayliss-Smith *et al.*, 1979; Healey *et al.*, 1981; Green *et al.*, 1986). The velocity asymmetry is ascribed to a sudden increase in tidal prism as the marsh surface is flooded, and to flow convergence to the creek during ebb (Bayliss-Smith *et al.*, 1979). Moreover, differential resistance coefficients for the channel and over-marsh portions of the flow attenuate the transient above-bankfull stage (French and Stoddart, 1992) favouring a shorter slack near high water and ebb dominance (Friedrichs and Perry, 2001). Often the ebb velocity exceeds the flood velocity (Bayliss-Smith *et al.*, 1979; Leopold *et al.*, 1993; Myrick and Leopold, 1963; Healey *et al.*, 1981; Green *et al.*, 1986), but this is not a strict rule, since several tidal channels are flood-dominated particularly when the corresponding marsh areas are limited (Ayles and Lapointe, 1996). In other cases peak flooding currents are, on average, stronger than ebb currents, but with peak ebb velocities maintained for a longer period of time (Leonard *et al.*, 1995).

Furthermore, tidal channels tend to have stable planforms, and channel migration seems to be consistently slower than fluvial rivers, particularly in vegetated marshes (Gabet, 1998). Bank migration is produced by block collapse through a combination of cantilever and toppling failures (Allen, 1989), and low rates of lateral migration are due to the persistence of failed bank material, which temporarily protects the bank from erosion (Gabet, 1998). Lateral migration also decreases after sediment deposition on the marsh surface, which reduces tidal prism and flow velocity in the creeks (French and Stoddart, 1992). Because of this slow migration and frequent marshplain flooding and deposition, salt-marshes evolve differently from terrestrial floodplains. In floodplains, the amount of sediment reworked by river migration is consistently greater than the sediment deposited by overbank flow whereas in salt-marshes the opposite is true (see Howard, 1996).

Terrestrial rivers often have a characteristic asymmetry of meander planform which is termed bend skewing and produces the typical gooseneck loops (Carson and LaPointe, 1983). The cause of this asymmetry is generally hypothesized to be the delay between the channel curvature maximum and the water velocity maximum at the bank, which is responsible for bank erosion (Parker *et al.*, 1983). This theory is supported by computer models of river meandering that evolve gooseneck loops (Sun *et al.*, 1996; Howard and Knutson, 1984).

Current theories of meander evolution have been developed for terrestrial channels where the flow is unidirectional, and may not be strictly appropriate for tidal channels due to the characteristic bidirectionality of the tidal flow. For example, an initial sinusoidal planform (Figure 1A) will develop asymmetric gooseneck loops due

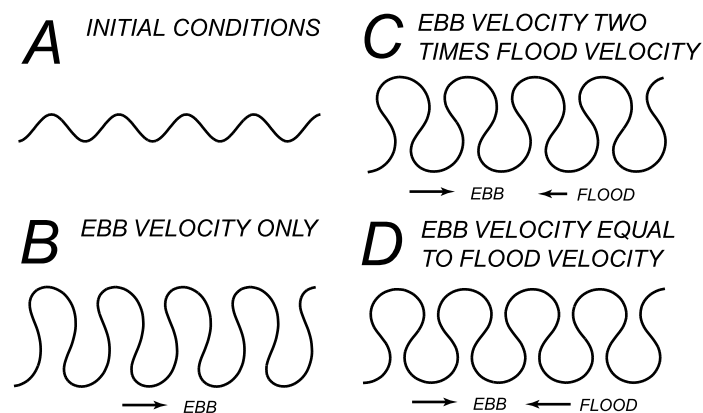


Figure 1. Possible evolution patterns of salt-marsh meanders

to unidirectional flow (Figure 1B). Under the influence of bidirectional flow, meanders should evolve differently, producing a distinctive planform morphology. In ebb-dominated tidal creeks, skewing of bends should still be recognizable, although somewhat subdued (Figure 1C). In situations where the ebb flood velocities are similar, meanders should become symmetrical (Figure 1D). The situation is complicated by the high variability of the flow in a creek and related sediment transport, which are affected by both tidal regime and storm frequency (Leonard *et al.*, 1995). For example Bayliss-Smith *et al.* (1979) recorded a flood velocity peak greater than the ebb peak during a storm tide, for a tidal creek normally ebb-dominated during fair-weather. This hydrodynamic complexity hinders the determination of the dominant morphological flow (*sensu* Wolman and Miller, 1960), and its direction (i.e. if it occurs during ebb or flood).

The scope of this paper is the identification, by studying the geometrical characteristics of tidal meanders, of the direction of the dominant flow producing tidal meanders.

STUDY AREA AND SURVEY METHODS

The focus of our study is a tidal channel located in China Camp Marsh in Marin County, California (Figure 2). (see also Gabet, 1998). The tidal regime is semidiurnal, with an excursion of 2 m during spring tide. Marsh sediments range from fine silts to clays, with shell fragments on the channel bottom. Two plant species dominate the marsh: *Spartina foliosa* Trin. (cordgrass) grows on the channel banks and point bars and can withstand long periods of inundation; *Salicornia virginica* L. (pickleweed) covers 90 per cent of the marsh plain. Significant progradation of the marsh began in 1850 when a pulse of sediment, from hydraulic mining operations in the Sierra Nevada, was delivered to the San Francisco Bay by the Sacramento River (Gilbert, 1917). As a consequence, the channel studied here has a relatively straight reach through the recently accreted portion of the marsh, since meanders have not had enough time to develop.

The channel banks were surveyed with a Total Station to create a channel planform base-map (Figure 3). Eighteen channel cross-sections were surveyed in April 1995 (Figures 3 and 4) with a Kern level, stadia rod, and tape. Slump blocks, signs of active bank erosion, were identified in the field and mapped onto the base-map.

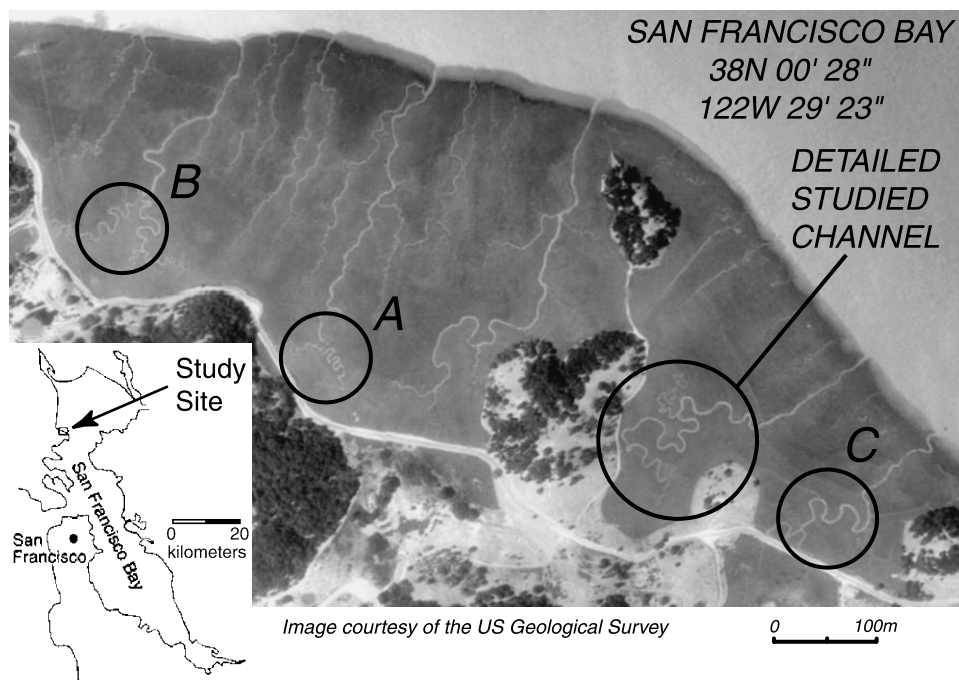


Figure 2. Channel location at China Camp Marsh in the San Francisco Bay, California. The letters A, B, and C refer to three other groups of tidal meanders examined

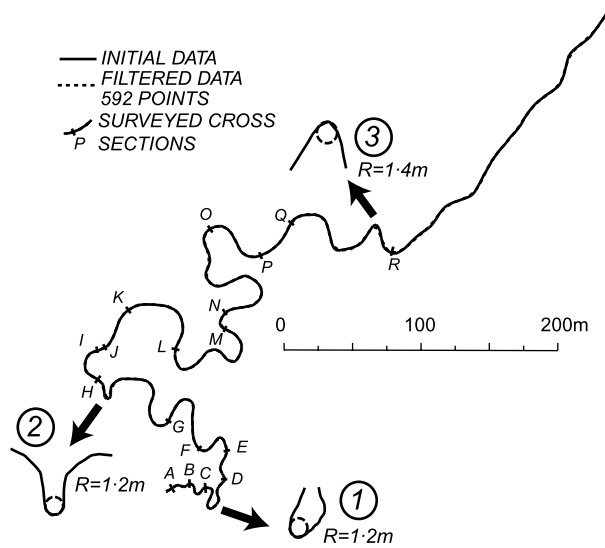


Figure 3. Channel axis plot (solid line) and location of the surveyed cross-sections (capital letters). The dotted line is the resulting channel axis after smoothing with a Savitzky-Golay filter. Three test bends with high curvature are indicated as well as the corresponding curvature calculated by inscribing a circle in the channel path

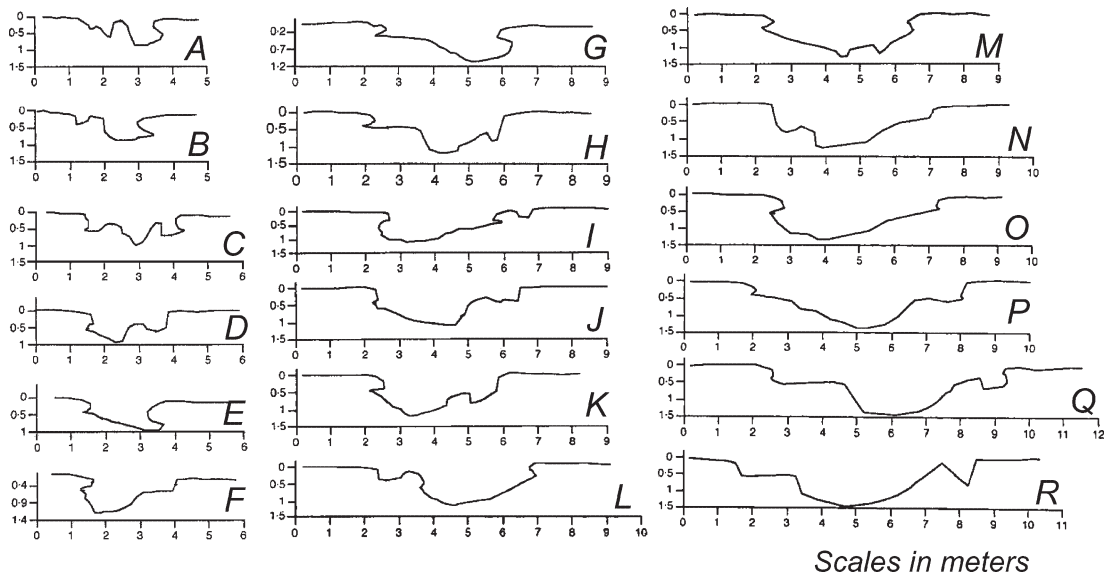


Figure 4. Surveyed cross-sections. View is downstream (bayward). Elevations are relative to the local marsh plain elevation designed as zero elevation for each cross-section

Furthermore, a comparison with other tidal meanders in the same marsh was carried out with data extracted from aerial photographs (locations A, B and C in Figure 2).

CHANNEL CURVATURE EXTRACTION FROM FIELD DATA

Curvature plays a fundamental role in meander formation and migration (Ikeda *et al.*, 1981). The extraction of curvature values from channel planforms is inherently difficult. For example, consider a circle having a radius equal to one (Figure 5). The corresponding curvature is then constant and equal to -1 . If we introduce a small

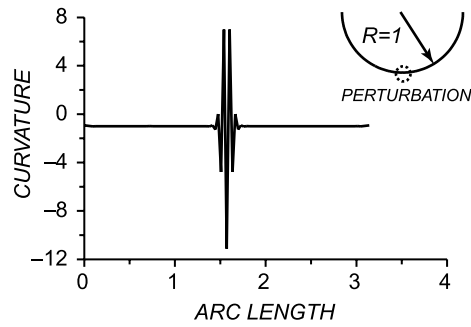


Figure 5. Curvature extraction of a circle with a three points stencil. A small perturbation in the coordinates of the circle creates significant oscillations in the curvature values

perturbation in the circle's coordinates, the consequences for the curvature are significant. In Figure 5 the values of the ordinates of two points of the circle are changed by only 1/1000 of their original value. As a consequence, curvatures in the neighborhood of the two points are characterized by strong oscillations, with maximum values eleven times the original one (Figure 5). In this example the algorithm we applied for curvature extraction utilizes three consecutive points on the curve. The algorithm finds the circle passing for three consecutive points and derives the curvature from the corresponding radius. After the perturbation is introduced, the modified points define a smaller circle, having a higher curvature value. The sensitivity of the curvature algorithm can be decreased by forcing more than three consecutive points to belong to the same circle. Data filtering is thus necessary for curvature extraction and the choice of an adequate filter technique is critical.

The raw data are a set of surveyed channel axis coordinates. The coordinates are unevenly spaced but fully describe the channel pattern (solid line in Figure 3). We applied a cubic spline interpolation for the x - and y -coordinates (Davis, 1986; De Boor, 1978). In this way each channel axis point is determined by two 3 third order polynomials:

$$\begin{aligned} x(s) &= \alpha_1^{(k)} + \alpha_2^{(k)}s + \alpha_3^{(k)}s^2 + \alpha_4^{(k)}s^3 \\ y(s) &= \beta_1^{(k)} + \beta_2^{(k)}s + \beta_3^{(k)}s^2 + \beta_4^{(k)}s^3 \end{aligned} \quad (1)$$

where s is a curvilinear coordinate. The eight parameters α_i and β_i have different values for each segment k between two consecutive points. Their value is determined by the coordinates of the two segment extremes as well as by imposing continuity of first and second derivatives between consecutive segments.

The curvature is calculated as:

$$C = \frac{\left[\frac{dx}{ds} \frac{d^2y}{ds^2} - \frac{dy}{ds} \frac{d^2x}{ds^2} \right]}{\left[\left(\frac{dx}{ds} \right)^2 + \left(\frac{dy}{ds} \right)^2 \right]^{3/2}} \quad (2)$$

This formula has the advantage of keeping the sign of the curvature, which is positive (negative) when the bend is turning right (left) for increasing values of s .

The spline interpolation may be also utilized to resample the channel axis points. From Equation 1, the arc length of each segment is determined by:

$$s'(s) = \int_{s_0}^s \sqrt{\left(\frac{dx}{ds} \right)^2 + \left(\frac{dy}{ds} \right)^2} ds \quad (3)$$

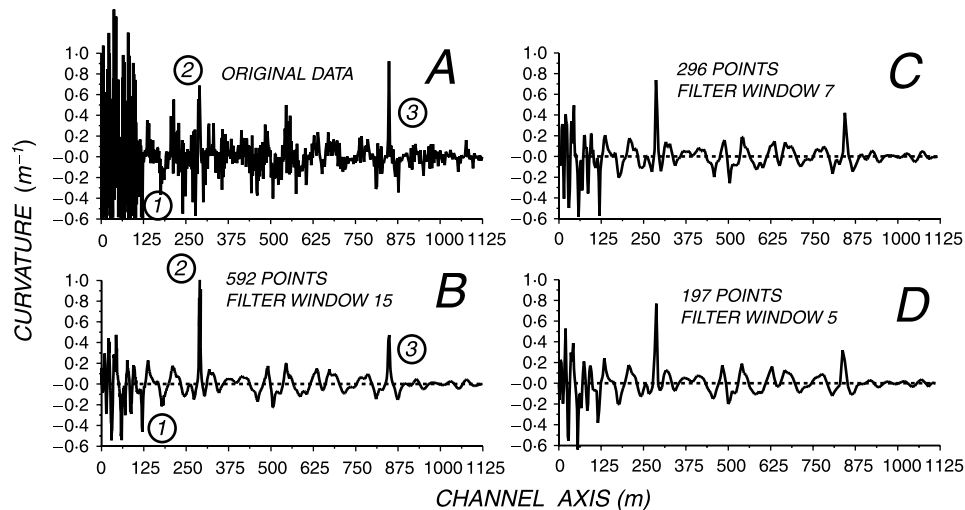


Figure 6. Channel curvature as a function of the channel axis coordinate. (A) Original data. (B) Original data filtered with a Savitzky-Golay filter and a data window of 15 points; the three circled numbers refer to the high curvature locations displayed in Figure 3. (C) Subset of the original data filtered with a data window of seven points. (D) Subset of the original data filtered with a data window of five points

where s_0 is the starting point of the channel. Integration of Equation 3 is performed with the Simpson's rule, which is exact for polynomials of degree 3 (Press *et al.*, 1992). A new set of points equally spaced on the curve is thus calculated, and the parameters of the spline interpolation for these new segments are recalculated as in Equation 1, where the generic curvilinear coordinate s is replaced by the arc length s' .

The curvature thus obtained may be plotted against the distance along the channel axis (Figure 6A). The resulting plot is characterized by high frequency oscillations, as in the example in Figure 5, making further analysis of the data difficult. A suitable filter (low-pass) is then applied. An appropriate low-pass filter will eliminate most of the high frequency noise without excessively damping curvature values in highly sinuous reaches while preserving the essential geometry of the planform.

In Figure 3, three 'test' points are identified, where the curvature is particularly high. A value for the curvature is calculated by inscribing a circle in the channel axis pattern. After filtering, we evaluate whether the value of the curvature at these locations is preserved or not. We apply the Savitzky-Golay low-pass filter (Hamming, 1983), to the x and y coordinates separately. The filter replaces each coordinate with a local average of neighbouring points in a moving window:

$$x_i^{\text{filtered}} = \frac{1}{2k+1} \sum_{j=-k}^k a_{i+j} x_{i+j} \quad (4a)$$

$$y_i^{\text{filtered}} = \frac{1}{2k+1} \sum_{j=-k}^k a_{i+j} y_{i+j} \quad (4b)$$

with $(x_i^{\text{filtered}}, y_i^{\text{filtered}})$ the coordinates of the i point after filtering, a_j the average coefficients, and $2k+1$ the number of points involved in the averaging process (filter window).

The coefficients of this average are calculated so that the underlying function in the moving window is a polynomial of high order. The filter moves the coordinates of the channel axis and tries to force several of them (depending on the window size) to stay on a polynomial curve. The application of the filter to the coordinates rather than the curvature has the advantage of directly producing the modified channel planform, which can then be compared to the original planform. Optimal filtering is achieved with a fifth order polynomial filter and a filter window of 15 points applied three times. It is interesting to note that the window length is similar to the average

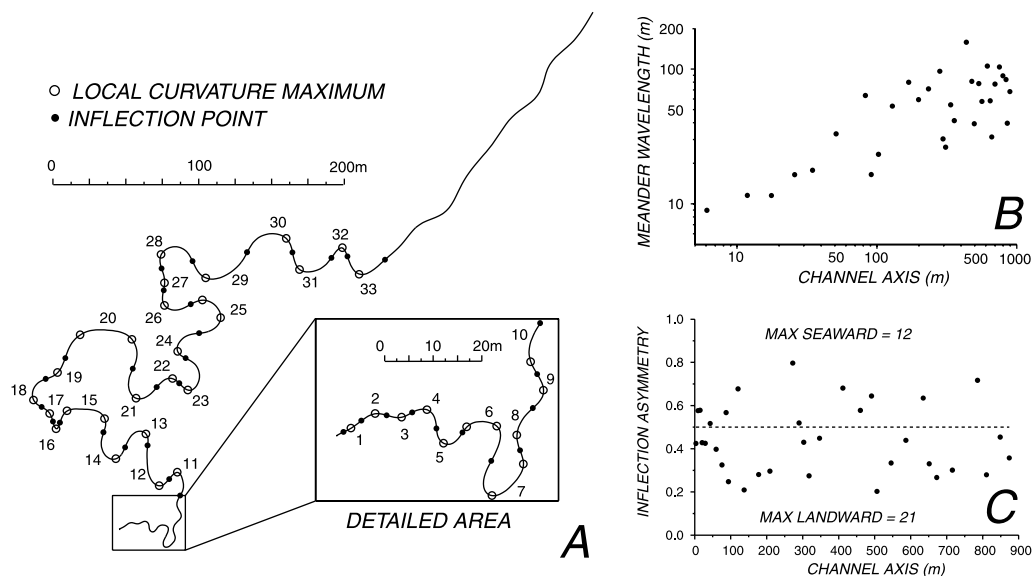


Figure 7. (A) Location of inflection points and curvature maxima on the channel axis. Each bend is numbered from 1 to 33. (B) Meander wavelength (twice the distance between two inflection points along the axis coordinate) as a function of channel axis coordinate. (C) Inflection asymmetry as a function of channel axis coordinate. The dotted line represents the situation when the curvature maximum is at the midpoint of the bend

bend length. The final planform is essentially identical to the original one (Figure 3). The decrease in the curvature values at the three test points is minimal, suggesting a reasonable balance between reduction of the high frequency noise and preservation of curvature peaks. The final curvature distribution crosses the zero value only once every channel bend, further validating the filtering and smoothing technique (Figure 6B).

We then assess the stability of our approach by evaluating whether changes in the distance between axis coordinates affect curvature distribution. The filter described above is applied to two new sets of points. The first set is derived from the original x and y coordinates considering every other point only. The second considers only every third point of the original set. The filter is again based on a fifth order polynomial and the number of points in the moving average is reduced in order to maintain a constant window length. Resulting curvature plots are similar, thus confirming the stability of the method (Figure 6C, D).

The curvature distribution in Figure 6B allows rapid identification of each meander bend, defined as the channel reach between two points with zero curvature (inflection points). We identify 33 bends (Figure 7A), and locate the curvature maximum (or maxima) in each bend. Although two consecutive bends seldom have the same length, the local meander wavelength along the curvilinear coordinate can be calculated as twice the bend length. Meander wavelengths increase with distance downstream, from 10 m near the channel head to 150 m for reaches closer to the mouth (Figure 7B). These data suggest a possible log–log relationship between wavelength and distance from the channel head. The asymmetry of each meander is determined by calculating the distance between the curvature maximum and the inflection points:

$$\text{Inflection asymmetry} = \frac{s_{\max} - s_1}{s_2 - s_1} \quad (5)$$

where, for each bend, s_1 and s_2 are the curvilinear coordinates of the upper and lower inflection point, and s_{\max} the coordinate of the curvature maximum within the bend.

The meander is asymmetric if the curvature maximum is not located near the bend midpoint, but is closer to the upper or lower inflection point. When the bend has multiple apices, the absolute maximum is considered.

This definition is similar to the delayed-inflection asymmetry introduced in Carson and LaPointe (1983), but the identification of a channel transverse is more objectively done considering the curvature maxima of two consecutive bends, without defining any 'valley' direction. In terrestrial rivers, the maximum is closer to the upstream inflection point, a direct consequence of the river flowing downstream (Parker *et al.*, 1983). From our data the tidal creek shows a similar behavior. Sixty-four per cent of the bends have a landward inflection point, indicating that the flow is ebb dominated (Figure 7C). In particular bends 7, 12, 13, 14, 23 and 24 in Figure 7A are skewed in the direction of the ebb flow. The remaining bends, with seaward inflection point, have on average a smaller inflection asymmetry, and testify to the complexity of the processes that shape tidal meanders. As in rivers, the complex evolution of channel bends, together with differences in local sediment characteristics, marsh platform gradients, and boundary conditions, seldom produce a regular train of meanders. Thus every result is only statistically significant. To further collaborate our findings we applied the filtering and curvature calculations to segments of three other channels, where regular and well developed meanders are present (locations A, B, and C in Figure 2). For these, the channel axis coordinates were derived directly from aerial photographs (Figure 2).

Plots of the curvature as a function of channel axis show again that the absolute maximum in each bend is closer to the landward inflection point, evidence of ebb domination (Figure 8). Most of the bends also have two local curvature maxima, with the greater always landward. Although some isolated bends have a flood inflection asymmetry, we did not find any group of meanders skewed in the flood direction.

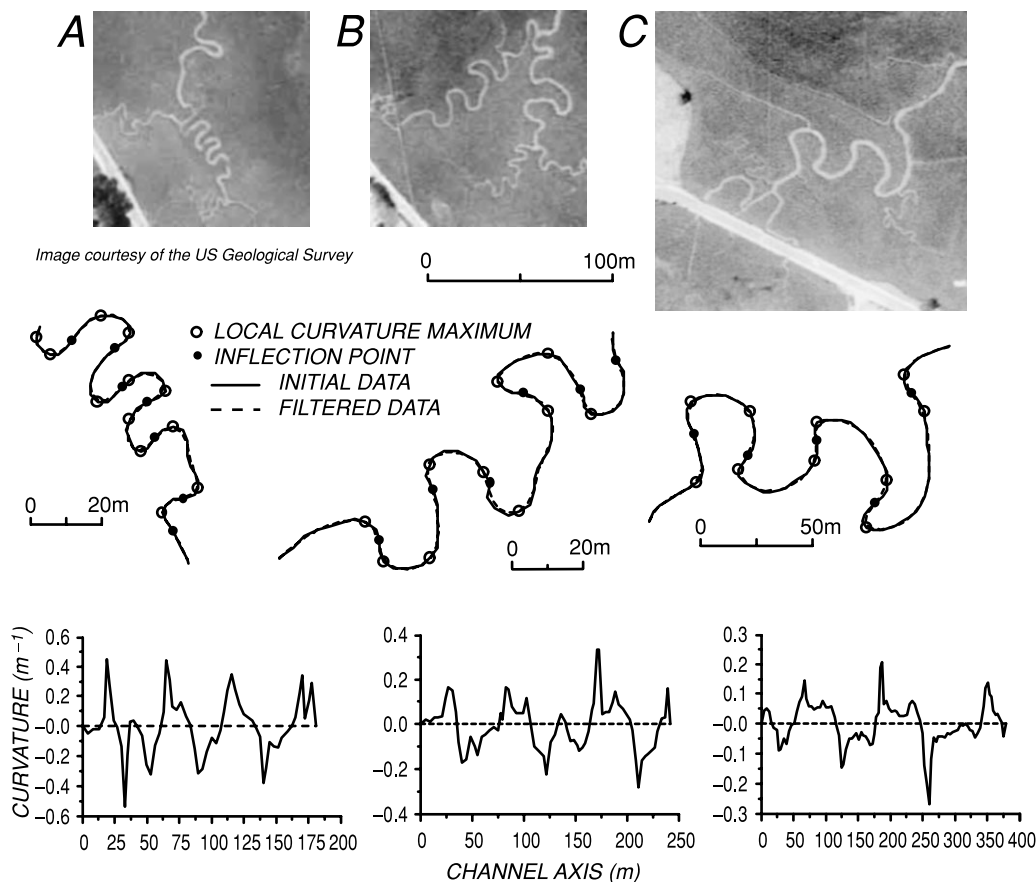


Figure 8. Curvature as a function of channel axis, inflection points, and curvature maxima for the three groups of meanders indicated in Figure 1 (locations A, B, and C)

LOCATION OF BANK EROSION IN TIDAL CHANNELS

To model the effects of bidirectional flow on bank erosion in tidal channels, we adopt the Johannesson and Parker (JP) model (Johannesson and Parker, 1989). In the JP model, extensively applied in terrestrial rivers, the flow is considered at bankfull, which corresponds to the dominant discharge (Leopold and Maddock, 1953). In salt-marshes both flood and ebb maxima, considered as ‘formative events’ (Bayliss-Smith *et al.*, 1979; French and Stoddart, 1992), occur for elevations different from bankfull (higher than bankfull during flood and lower during ebb). The JP model can be extended to flows that are not at bankfull, provided that: (a) the flow is unidimensional; (b) the channel width and depth are almost constant along a meander wavelength; (c) in each instant the discharge is to a first approximation constant along a channel bend. However, the discharge can be changed in time to account for the unsteady characteristics of the flow. These hypotheses are, to a first approximation, also valid for tidal meanders.

Despite the fact that the flow field during over-marsh tides has a tridimensional structure it is still possible to consider the flow as predominantly unidimensional in the channel, since the velocities on the marsh surface are one order of magnitude smaller (Christiansen *et al.*, 2000; Lynn *et al.*, 1995). Furthermore the effects of channel widening and deepening as well as variations in discharge are considered negligible at the bend scale. From field data, channel widening and deepening can be approximated by an exponential law (Figure 9A, B) (Lanzoni and Seminara, 1998; Friedrichs and Aubrey, 1994):

$$w = w_0 \exp(s/L_w) \quad (6a)$$

$$h_{MAX} = h_0 \exp(s/L_h) \quad (6b)$$

where h_{MAX} is the maximum channel depth in the cross-section, w is the channel width, and h_0 and w_0 are depth and width, respectively, at the channel head. L_h and L_w are length scales which determine the rate of widening and deepening, respectively, and are estimated from Figure 9A, B. The values for these parameters are shown in Table I. From the shape of the cross-sections, we assume that the average depth h is half the maximum depth h_{MAX} . The relative width and depth changes at the bend scale are:

$$\epsilon_w = \frac{\lambda}{w} \frac{dw}{ds} = \frac{\lambda}{L_w} = 0.01 \div 0.16 \quad (7a)$$

$$\epsilon_h = \frac{\lambda}{h} \frac{dh}{ds} = \frac{\lambda}{L_h} = 0.006 \div 0.09 \quad (7b)$$

where λ is the meander wavelength. Thus, the width increases faster than the depth.

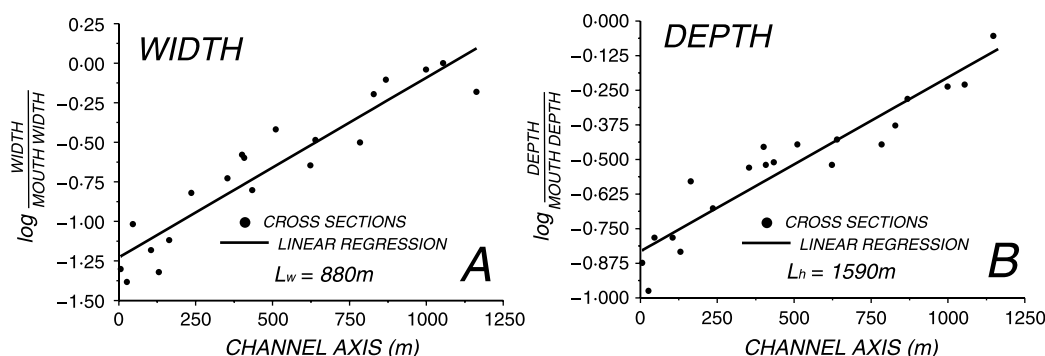


Figure 9. Semilogarithmic plot of channel width (A) and channel depth (B) versus channel axis coordinate

Table I. Model parameters

Parameter	w	h_{MAX}	h	$L_w(m)$	$L_h(m)$	$w_0(m)$	$h_0(m)$	A	$u_0(m\ s^{-1})$	K_f	A'
Value	$w_0 \exp(s/L_w)$	$h_0 \exp(s/L_h)$	$0.5h_{MAX}$	900	1600	2.2	0.75	6	$c. 0.6^*$	$c. 0.016^{**}$	$130(2h/w)^2$

Source: * Pestrong (1965), Leopold *et al.* (1993); ** Defina (2000), Collins *et al.* (1998)

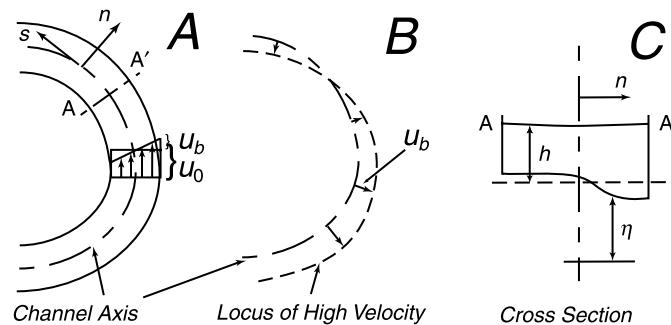


Figure 10. Definition diagrams. (A) Meandering tidal channel. (B) Bank velocity increment u_b and locus of high velocity. (C) Channel cross-section A–A'

A further assumption, partially justified by field data (Pestrong, 1965; Myrick and Leopold, 1963), is that the peak velocity is uniform along the entire channel for both ebb and flood flows. This implies that the channel cross-section adjusts itself to an increasing discharge in order to maintain an almost constant maximum velocity. To account for the inherent variability of tidal flow in a channel, emphasized by the discontinuous prism-stage relation (Healey *et al.*, 1981), different discharges will be utilized in the model.

The model considers a channel with a reach-averaged (i.e. over a meander wavelength) tangential velocity u_0 and depth h (Figure 10A, C). Moreover the channel axis curvature radius is considered large with respect to the channel width. Because of the secondary current triggered by the channel curvature, the momentum is redistributed in the channel cross-section with a velocity increase in the outer bank of a bend. As a consequence, the outer bank is eroded and sediment is deposited on the point bar in the inner bank. The increase of velocity in the outer bank can be described, at first order, by a term having value u_b at the bank which can be added to the average velocity u_0 (Figure 10A). The value of u_b is plotted normal to the channel axis on the side of the channel where the velocity is higher. The corresponding set of points determined by the terminus of the velocity vector u_b defines the locus of high velocity (Figure 10B).

As hypothesized by Ikeda *et al.* (1981) and confirmed by field data (Pizzuto and Meckelnburg, 1989), the bank erosion can be set proportional to the difference u_b between bank velocity and averaged velocity u_0 through the equation:

$$E = ku_b \quad (8)$$

where E ($m\ s^{-1}$) is the lateral erosion rate acting normal to the channel axis and k is a non-dimensional coefficient of proportionality, determined in the field. Because of Equation 8, the locus of high velocity determines the areas of higher bank erosion, and coincides with the new channel axis after bank erosion and slump block removal is accomplished (Figure 10B).

Following Johannesson and Parker (1989), the simplification of the shallow water equations leads to the following relationship:

$$u_0 \frac{\partial u_b}{\partial s} + 2 \frac{u_0}{h} K_f u_b = \frac{w}{2} \left[-u_0^2 \frac{\partial C}{\partial s} + K_f C \left(\frac{u_0^4}{gh^2} + (A + A' - 1) \frac{u_0^2}{h} \right) \right] \quad (9)$$

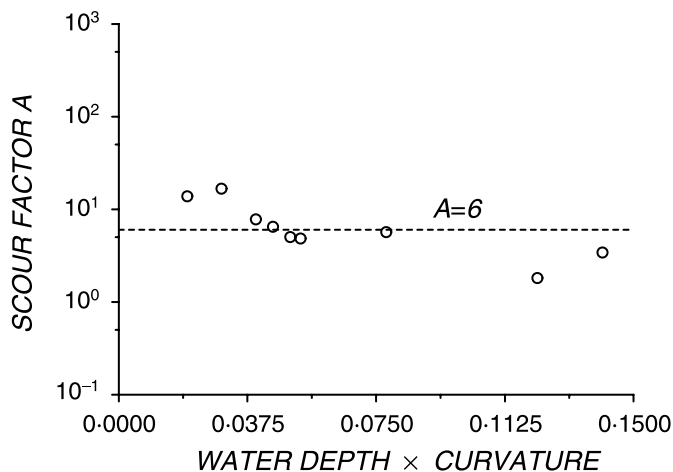


Figure 11. Scour factor estimation

where u_0 is the average flow velocity, u_b is the velocity increment at the bank with respect to u_0 , K_f is a friction coefficient, C is channel curvature, A is a scour factor which depends on the transverse slope of the bottom in the channel bends, and A' is an additional constant which accounts for the momentum redistribution caused by the secondary current (Johannesson and Parker, 1989). At a cross-section, the transverse bed slope is linked to the channel curvature. The parameter A in Equation 9 accounts for this link and is calculated through the following relationship (Ikeda *et al.*, 1981):

$$A = \frac{1}{Ch} \frac{\eta(n)}{n} \quad (10)$$

where n is the coordinate in the direction perpendicular to the channel axis and η is the channel bed elevation from a reference level (Figure 10C). From the cross-sections survey (Figure 4), we can determine the parameter A by plotting the value of transverse bed slope against the product of curvature and water depth for each cross-section (Figure 11). The resulting data are scattered because of the inherent difficulty in calculating the transverse slope of the highly irregular bed (see Figure 4). In the following simulations, we adopt a value $A = 6$, corresponding to the averaged value in Figure 11.

With the friction coefficient and the ratio between half width and depth ($\gamma = w/2h$), A' can be evaluated with the equation (Johannesson and Parker, 1989):

$$A' = 181 \frac{2\chi^2 + \frac{4}{5}\chi + \frac{1}{15}}{\gamma\chi_1} \quad (11)$$

where:

$$\chi_1 = \frac{K_f^{-1/2}}{13}, \quad \chi = \chi_1 - \frac{1}{3}, \quad \gamma = \frac{w}{2h} \quad (12)$$

The value of A' is reported in Table I. The width to depth ratio in this channel is consistently smaller than in terrestrial rivers and increases towards the mouth (see also Gabet, 1996), therefore, from Equation 11, it follows that the parameter A' is higher than in terrestrial rivers. We modify the JP model to consider two flows acting one after the other, the first with constant maximum ebb velocity from the inland reaches to the channel mouth, the second with constant maximum flood velocity from the channel mouth to inland. The reduction of the tidal hydrodynamics to only two peak velocities is justified by the assumption that only peak velocities have a

geomorphological impact. The same assumption is the basis for several studies in terrestrial rivers, where a uniform flow is considered instead of a propagating flood wave (Ikeda *et al.*, 1981; Blondeaux and Seminara, 1985; Johannesson and Parker, 1989). The model predicts the location where bank failure is likely to occur, corresponding to the locations of high u_b . To account for the intrinsic variability of the flow in a creek, which depends upon tidal oscillations and storm surges, we run the model with different values of the ebb and flood discharges. Results show that the intensity of the bank velocity u_b strongly depends on the value of the discharge utilized; but that the locations where bank failure is likely to occur (i.e. the banks of the channel where the velocity is higher) are almost independent of flow intensity.

We present results for ebb flow (inland to mouth) and flood flow (mouth to inland), both characteristic of tidal creeks. In both cases, bank velocities are out of phase with curvature (Figure 12). We note that the high velocity core reported in Figures 12 and 13 does not refer to a single tidal cycle (a unique value of discharge), but is the typical averaged distribution of bank velocity for any flow in the creeks (with intensity depending on flow discharge). Since bank failures in vegetated salt marsh channels produce slump blocks that persist in the channel

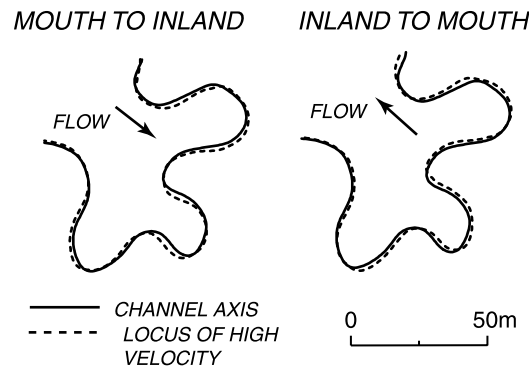


Figure 12. Channel axis (solid line) and path of high velocity core (dotted line) for mouth to inland (flood) and inland to mouth (ebb) flow. The locations of the two plots are the same and correspond to bends 21–25 in Figure 7A

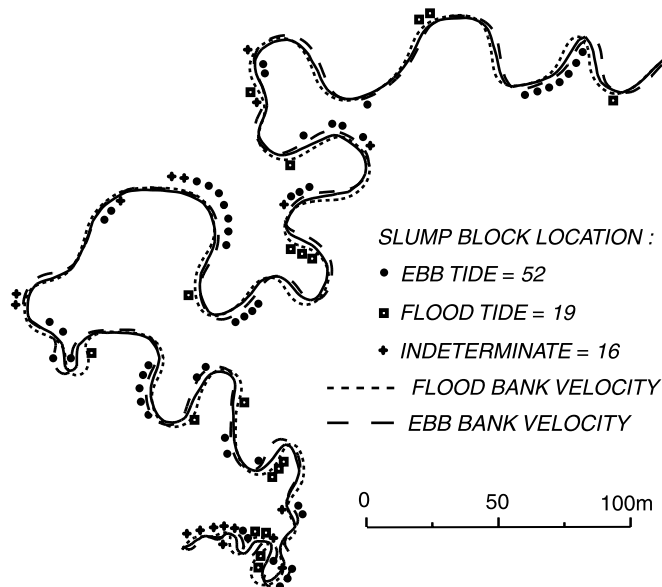


Figure 13. Map of slump blocks locations detected by field survey and locus of near-bank velocity (both for ebb and flood flow) determined after model simulations

for several years, it is possible to identify reaches of active bank erosion and test model predictions. Locations of slump blocks, mapped in the field, are compared to model simulations, clearly indicating that channel migration is predominantly ebb-driven (Figure 13). A similar conclusion is reached by comparing slump block locations and curvature maxima (Figure 7A). Most of the blocks are located after the curvature peak, further supporting the model findings.

The dominance of the ebb flow in determining planform morphology may be due to higher velocities on the ebb flow than on the flood flow. Velocity data collected during a full tidal cycle on 13 March 2001 (spring tide) at cross-section L on Figure 4 show a maximum ebb velocity equal to 0.32 m s^{-1} and a maximum flood velocity equal to 0.17 m s^{-1} . These limited data suggest that the creek is probably ebb-dominated, partly confirming the results obtained from the planimetric data. Ebb-dominated channels were also reported in San Francisco Bay by Leopold *et al.* (1993) and Pstrong (1965). In this study, we are applying an evolution model based on theoretical results valid for rivers. Bidirectional flow, however, is not the only difference between salt-marsh creeks and terrestrial rivers, and the following points can be considered in the future to improve the JP model in tidal environments. Tidal channel discharge increases toward the mouth because the channel drains an increasingly wide salt-marsh surface (Rinaldo *et al.*, 1999a,b). As a direct consequence, channel cross-section changes and the channel becomes deeper and wider. Discharge in terrestrial rivers also increases downstream, but in salt marsh channels discharge variations are much bigger, occurring over a relatively small channel length. The flow can be considered unidimensional only when it is confined in the channel. When the water invades the salt-marsh surface (during flood) or the channel drains the marsh surface (during ebb) a complex three-dimensional flow field results. This is particularly true for the flood peak velocity, which often happens for water levels higher than salt-marsh elevation. Ebb peak is instead more likely occurring when water elevations are less than bankfull (Myrick and Leopold, 1963; Bayliss-Smith *et al.*, 1979). In contrast to terrestrial rivers, where overbank flow is linked to rare flood events, marsh plain flooding occurs relatively often.

Furthermore, in tidal environments it is not possible to define a basic uniform flow directly related to the channel bottom slope; the flow is instead determined by the periodicity of the tidal forcing. Finally, sediment is not conserved along the channel since a consistent fraction is carried and deposited on the salt-marsh surface during high tide.

CONCLUSIONS

In this investigation, field surveys were used to characterize the channel planform of a tidal channel at China Camp Marsh in the San Francisco Bay, California. To model the planform evolution, we assume that the topographic curvature of the channel centreline is a key element driving meander migration. Coordinates for the channel were determined from a high-resolution survey and a cubic spline interpolation in the x - and y -directions is utilized to calculate the continuous distribution of axis curvature. The resulting curvature signal, however, needs to be filtered, since small variations in axis location produce amplified peaks when the curvature is calculated with three consecutive points on the channel axis. For this purpose, we utilized a low-pass filter (Savitzky-Golay) in the x - and y -directions.

The filter forces consecutive points to stay on a polynomial curve of order n , thus smoothing oscillations. The application of the filter to the coordinates rather than to the curvature has the advantage of directly producing the modified shape of the channel after smoothing. By comparing the smoothed planform to the original, we were able to evaluate whether the smoothing process was too severe. We found an optimal filter with a fifth-order polynomial applied to a 15-point window.

We then investigated the asymmetry of the meander planform. Terrestrial rivers, because of the delay between the channel curvature maximum and the water velocity maximum at the bank, have skewed meander bends. This asymmetry in bend morphology stems from the hydrodynamics of unidirectional flow.

There is skewing where the curvature maximum of the bend is not located in the middle of two inflection points, but is closer to the upper or lower inflection point. In terrestrial rivers, the maximum is closer to the upstream inflection point, a direct consequence of the river flowing downstream. From our data, tidal creeks show a similar behaviour. The maximum in curvature is statistically closer to the landward inflection point, suggesting that the flow is ebb-dominated.

The curvature calculations, combined with data from numerous cross-sections along the tidal channel and an estimate of flow velocity and bottom friction, were utilized to parameterize a computer model.

Meander migration occurs through bank failure that is linked to flow velocity at the bank. The model predicts this velocity and, consequently, the location where bank failure is likely to occur. We present results for ebb flow (inland to mouth) and flood flow (mouth to inland), a unique characteristic of tidal creeks. In both cases bank velocities are asymmetrical with respect to curvature. Bank failures in vegetated salt-marsh channels are characterized by slump blocks that persist in the channel for several years. It is therefore possible to identify reaches of active bank erosion and test model predictions. The position of the slump blocks, determined in the field, were compared to model simulations, indicating that channel migration is predominantly ebb-driven. This result is in agreement with velocity measurements in salt-marsh channels in San Francisco Bay, indicating that the ebb velocity peak is greater than the flood peak. Finally, this study suggests that the relative velocities of the ebb and flood flows can be remotely determined by a simple analysis of the planform geometry.

REFERENCES

- Ahnert F. 1960. Estuarine meanders in the Chesapeake Bay area. *The Geographical Review* **50**: 390–401.
- Allen JRL. 1989. Evolution of salt-marsh cliffs in muddy and sandy systems: a qualitative comparison of British west-coast estuaries. *Earth Surface Processes and Landforms* **14**: 85–92.
- Ayles CP, Lapointe MF. 1996. Downvalley gradients in flow patterns, sediment transport and channel morphology in a small macrotidal estuary: Dipper Harbour creek, New Brunswick, Canada. *Earth Surface Processes and Landforms* **21**(9): 829–842.
- Barwis JH. 1978. Sedimentology of some South Carolina tidal-creek point bars, and a comparison with their fluvial counterparts. In *Fluvial Sedimentology*, Miall AD (ed.). Canadian Society of Petroleum Geologists. 129–160.
- Bayliss-Smith TP, Healey R, Lailey R, Spencer T, Stoddart DR. 1979. Tidal flows in salt-marsh creeks. *Estuarine and Coastal Marine Science* **9**: 235–255.
- Blondeaux P, Seminara G. 1985. A unified bar bend theory of river meanders. *Journal of Fluid Mechanics* **157**: 449–470.
- Carson MA, LaPointe MF. 1983. The inherent asymmetry of river meander planform. *Journal of Geology* **91**(1): 41–55.
- Christiansen T, Wiberg PL, Milligan TG. 2000. Flow and sediment transport on a tidal salt marsh surface. *Estuarine Coastal and Shelf Science* **50**(3): 315–331.
- Collins MB, Ke X, Gao S. 1998. Tidally-induced flow structure over Intertidal flats. *Estuarine, Coastal and Shelf Science* **46**: 233–250.
- Davis JC. 1986. *Statistics and Data Analysis in Geology*. Wiley: New York.
- De Boor C. 1978. *A Practical Guide to Splines*. Springer-Verlag: New York.
- Defina A. 2000. Two-dimensional shallow flow equations for partially dry areas. *Water Resources Research* **36**(11): 3251–3264.
- Fagherazzi S, Furbish D. 2001. On the shape and widening of salt marsh creeks. *Journal of Geophysical Research Oceans* **106**(C1): 991–1005.
- Fagherazzi S, Bortoluzzi A, Dietrich WE, Adami A, Lanzoni S, Marani M, Rinaldo A. 1999. Tidal networks 1. Automatic network extraction and preliminary scaling features from DTMs. *Water Resources Research* **35**(12): 3891–3904.
- French JR, Stoddart DR. 1992. Hydrodynamics of salt-marsh creek systems – implications for marsh morphological development and material exchange. *Earth Surface Processes and Landform* **17**(3): 235–252.
- Friedrichs CT, Aubrey DG. 1994. Tidal propagation in strongly convergent channels. *Journal of Geophysical Research Oceans* **99**(C4): 8053–8053.
- Friedrichs CT, Perry JE. 2001. Tidal salt marsh morphodynamics, a synthesis. *Journal of Coastal Research Special Issue no. 27*: 7–38.
- Gabet EJ. 1996. *Lateral migration and cross-sectional morphology of a tidal channel in Marin County, California*. Master's thesis, UC Berkeley, Berkeley, CA.
- Gabet EJ. 1998. Lateral migration and bank erosion in a saltmarsh tidal channel in San Francisco Bay, California. *Estuaries* **4B**: 745–753.
- Geyl WF. 1976. Tidal neomorphs. *Zeitschrift für Geomorphologie* **20**(3): 308–330.
- Gilbert GK. 1917. *Hydraulic mining debris in the Sierra Nevada*. United States Geological Survey Professional Paper 105.
- Green HM, Stoddart DR, Reed DJ, Bayliss-Smith TP. 1986. Saltmarsh tidal creek hydrodynamics, Scolt head Island, Norfolk, England. In *Proceedings of the Iceland Coastal and River Symposium*, Reykjavik, Iceland, Sigbjarnarson G. (ed.). National Energy Authority: Reykjavik; 93–103.
- Hamming RW. 1983. *Digital Filters*. Prentice Hall: New York.
- Healey RG, Pye K, Stoddart DR, Bayliss-Smith TP. 1981. Velocity variations in salt marsh creeks, Norfolk, England. *Estuarine, Coastal and Shelf Science* **13**: 535–435.
- Howard AD. 1996. Modelling channel evolution and floodplain morphology. In *Floodplain Processes*, Anderson MG, Walling DE, Bates PD (eds). John Wiley and Sons: Chichester; 15–62.
- Howard AD, Knutson TR. 1984. Sufficient conditions for river meandering – a simulation approach. *Water Resources Research* **20**(11): 1659–1667.
- Ikeda S, Parker G, Sawai K. 1981. Bend theory of river meanders. 1. Linear development. *Journal of Fluid Mechanics* **112**: 363–377.
- Johannesson H, Parker G. 1989. Linear theory of river meanders. In *River Meandering*, Ikeda S, Parker G (eds). Water Resources Monographs, 12. AGU: Washington; 181–214.
- Lanzoni S, Seminara G. 1998. On tide propagation in convergent estuaries. *Journal of Geophysical Research Oceans* **103** (C13): 30793–30812.

- Leonard LA, Hine AC, Luther ME, Stumpf RP, Wright EE. 1995. Sediment transport processes in a west-central Florida open marine marsh tidal creek: the role of tides and extratropical storms. *Estuarine Coastal and Shelf Science* **41**: 225–248.
- Leopold LB, Maddock T. 1953. *The hydraulic geometry of stream channels and some physiographic implications*. US Geological Survey Professional Paper **252**.
- Leopold LB, Collins JN, Collins LM. 1993. Hydrology of some tidal channels in estuarine marshlands near San Francisco. *Catena* **20**: 469–493.
- Lynn AL, Hine AC, Luther ME. 1995. Surficial sediment transport and deposition processes in a *Juncus roemerianus* marsh, west-central Florida. *Journal of Coastal Research* **11**: 322–336.
- Myrick RM, Leopold LB. 1963. *Hydraulic geometry of a small tidal estuary*. US Geological Survey Professional Paper **422-B**.
- Parker G, Diplas P, Akiyama J. 1983. Meander bends of high amplitude, *Journal of Hydraulic Engineering – ASCE*, **109**(10): 1323–1337.
- Pestrong R. 1965. *The development of drainage patterns on tidal marshes*. Stanford University, Publications in Geological Science, Technical Report 10.
- Pizzuto JE, Meckelnburg TS. 1989. Evaluation of a linear bank erosion equation. *Water Resources Research* **25**(5): 1005–1013.
- Press WH, Teukolsky SA, Vetterling WT, Flannery BP. 1992. *Numerical Recipes in FORTRAN: the Art of Scientific Computing*. Cambridge University Press: New York.
- Rinaldo A, Fagherazzi S, Lanzoni S, Marani M, Dietrich WE. 1999a. Tidal networks 2. Watershed delineation and comparative network morphology. *Water Resources Research* **35**(12): 3905–3917.
- Rinaldo A, Fagherazzi S, Lanzoni S, Marani M, Dietrich WE. 1999b. Tidal networks 3. Landscape-forming discharges and studies in empirical geomorphic relationships. *Water Resources Research* **35**(12): 3919–3929.
- Seminara G, Tubino M. 1992. Weakly nonlinear theory of regular meanders. *Journal of Fluid Mechanics* **244**: 257–288.
- Sun T, Meakin P, Jossang T, Schwarz K. 1996. A simulation model for meandering rivers. *Water Resources Research* **32**(9): 2937–2954.
- Wolman MG, Miller JP. 1960. Magnitude and frequency of forces in geomorphic processes. *Journal of Geology* **68**: 54–74.
- van Veen J. 1950. Eb- en vloodschaarsystemen in de Nederlandse getijwateren (Ebb and flood channel systems in Dutch tidal waters). *T. Kon. Nederl. Aardrijkskundig Genootschap* **67**: 303–325 (Weaddensymposium: in Dutch with English summary).